^{95}Mo Magic Angle Spinning NMR at High Field: Improved Measurements and Structural Analysis of the Quadrupole Interaction in Monomolybdates and Isopolymolybdates

Jean-Baptiste d'Espinose de Lacaillerie,*,† Fabien Barberon,† Konstantin V. Romanenko,‡ Olga B. Lapina,‡ Laurent Le Pollès,§ Régis Gautier,§ and Zhehong Gan‖

Laboratoire de Physique Quantique, UMR CNRS SIEN 7142, Ecole Supérieure de Physique et de Chimie Industrielles, 10 rue Vauquelin, 75231 Paris Cedex 05, France, Boreskov Institute of Catalysis, Prospekt Lavrentiva 5, Novosibirsk 630090, Russia, Laboratoire de Chimie du Solide et Inorganique Moléculaire, UMR CNRS 6511, Ecole Nationale Supérieure de Chimie de Rennes, Institut de Chimie de Rennes, Campus de Beaulieu, 35700 Rennes, France, and National High Magnetic Field Laboratory, 1800 East Paul Dirac Drive, Tallahassee, Florida 32310

Received: April 15, 2005; In Final Form: May 27, 2005

In this study, ^{95}Mo quadrupole couplings in various molydbates were measured easily and accurately with magic angle spinning (MAS) NMR under a directing field of 19.6 T. The resonance frequency of 54 MHz was sufficiently high to remove acoustic ringing artifacts, and the spectra could be analyzed in the usual terms of chemical shift and quadrupolar line shapes. For monomolybdates and molybdite, the quadrupole coupling dominated the NMR response, and the quadrupole parameters could be measured with better accuracy than in previous lower field studies. Moreover, despite the low symmetry of the molybdenum coordination, the usefulness of such measurements to probe molybdenum environments was established by ab initio density functional theory (DFT) calculations of the electric field gradient from known structures. The experimental NMR data correlated perfectly with the refined structures. In isopolymolybdates, the resonances were shapeless and DFT calculations were impossible because of the large and low symmetry unit cells. Nevertheless, empirical but clear NMR signatures were obtained from the spinning sidebands analysis or the MQMAS spectra. This was possible for the first time thanks to the improved baseline and sensitivity at high fields. With the generalization of NMR spectrometers operating above 17 T, it was predicted that ^{95}Mo MAS NMR could evolve as a routine characterization tool for ill-defined structures such as supported molybdates in catalysis.

Introduction

The different structures and polyhedron arrangements in solid molybdates result in extensive distortions of the ideal MoO_4^{2-} tetrahedron and MoO_6^{6-} octahedron.[1] Consequently, inorganic molybdates are amenable to meaningful studies by spectroscopies probing the local environment of molybdenum such as neutron diffraction, Fourier transform infrared, Raman,[2] Mo K edge XAS,[3,4] and molybdenum NMR. The latter, however, have remained scarcely used in the solid state for, due to the quadrupolar nature (spins 5/2) and low gyromagnetic ratio (γ) of its NMR active isotopes, namely, ^{95}Mo ($-1.751\ 10^7$ rad s^{-1} T^{-1}) and ^{97}Mo ($-1.788\ 10^7$ rad s^{-1} T^{-1}),[5] molybdenum NMR suffers from a reduced sensitivity ($\propto\gamma^{7/4}$) and a low resonance frequency. Even at 11.7 T, the Larmor frequencies in the 32−33 MHz range result in extensive baseline distortion by acoustic ringing. However, ^{95}Mo and ^{97}Mo are not entirely unfavorable to NMR. Their natural abundance (15.92 and 9.55%, respectively) is not worse than other commonly studied nuclei such as ^{29}Si. Their longitudinal relaxation time is not excessively long (in the range of seconds to hundreds of seconds for insulators). They figure in the upper half of the low γ range (defined as comprising nuclei resonating below 40 MHz at 9.4 T, that is below ^{15}N). Finally, the quadrupole moments of ^{95}Mo (−22mB) and ^{97}Mo (255mB) are comparable to the ones of ^{17}O (−25.58 mB) and ^{27}Al (146.6 mB), respectively. NMR of Mo(VI) in the solid state is thus possible even under moderate fields if the sensitivity is enhanced using isotopic enrichment or specific pulse scheme such as sechinv,[6] while the dead time associated with acoustic ringing can be circumvented using a quadrupolar echo sequence or even QCPMG.[7] Indeed, considering the importance of molybdate chemistry, the feasibility of molybdenum solid state NMR has been periodically investigated in the past within the fields of inorganic chemistry,[8−12] materials science,[13−15] and catalysis.[16−20]

As high field (>17 T) spectrometers are now being serviced worldwide, the limitations associated with the low γ are expected to vanish, and it has been recognized that it is now time to revisit the potential of ^{95}Mo to identify the local structures of molybdates.[11] However, to our knowledge, apart from a study of Bryce and Wasylishen[21] of a piano stool complex at 18.8 T, no studies of Mo(VI) in the solid state by NMR at ultrahigh fields have been published to date. We thus report here on one-pulse, natural abundance ^{95}Mo solid state magic angle spinning (MAS) NMR spectra obtained at 54.2 MHz (19.6 T) for model bulk compounds of monomolybdates and isopolymolybdate salts. This was at an applied magnetic field (B_0) nearly triple what was used for similar studies in the '80s[16] and still nearly double what was available in the '90s.[17] The feasibility of multidimensional ^{95}Mo experiments is also demonstrated for the first time. Finally, the

* To whom correspondence should be addressed. E-mail: Jean-Baptiste.dEspinose@espci.fr.
† Ecole Supérieure de Physique et de Chimie Industrielles.
‡ Boreskov Institute of Catalysis.
§ Ecole Nationale Supérieure de Chimie de Rennes.
‖ National High Magnetic Field Laboratory.

10.1021/jp0519621 CCC: $30.25
Published on Web 07/02/2005

measured quadrupole parameters were confronted for some compounds to values computed with the full potential DFT-based (density functional theory) method implemented in the WIEN2k code.[22]

Materials and Methods

Materials. Monomolybdates were purchased from Aldrich (United States) [$BaMoO_4$, Li_2MoO_4, α-K_2MoO_4, $Na_2MoO_4 \cdot 2H_2O$, and $(NH_4)_2MoO_4$] or synthesized at the Boreskov Institute of Catalysis (Russia) ($PbMoO_4$, α-$ZnMoO_4$, and Cs_2MoO_4). α-Na_2MoO_4 was obtained by heating $Na_2MoO_4 \cdot 2H_2O$ overnight at 520 K. $CaMoO_4$ came courtesy of Prof. E. Payen (UST Lille, France). $Al_2(MoO_4)_3$ was purchased from Alpha Chemicals (United States). Polymolybdates [Ba_2CaMoO_6 and $(NtBu_4)_2Mo_6O_{19}$] came courtesy of Prof. E. Payen except for the heptamolybdate $\{[(NH_4)_6Mo_7O_{24}] \cdot 4H_2O\}$, which was purchased from Aldrich. MoO_3 was from Aldrich. The samples were ground to powder when necessary and used as such. X-ray diffraction (XRD) patterns were verified prior to NMR using a Philips XPert MPD diffractometer at the Cu Kα radiation. Ionic radii were taken from the WebElements database.[23] Bond lengths and angles were either taken directly from the articles solving the structures when available or recalculated using the crystallographic parameters with the CARIne Crystallography software.[24]

MAS NMR. The ^{95}Mo isotope was preferred over ^{97}Mo, because its quadrupole moment is roughly 11−12 times weaker, thus, although it has a longer magnetization recovery time,[14] it exhibits much sharper NMR line shapes. MAS NMR experiments were performed at 19.6 T on a Bruker DRX spectrometer in 4 mm zirconia rotors at the NHMFL in Tallahassee (FL). ^{95}Mo ($I = 5/2$) one-pulse experiments were performed spinning at 10 kHz with a selective pulse ($\pi/6$) duration of 2 μs ($\Omega_I/2\pi \sim 40$ kHz). The spectral width was 100 kHz with digital filtering. Numbers of acquisitions for each sample are indicated in the figure captions, and recycle times are indicated in the tables. The chemical shift was referred to the resonance of a 1.5 M Na_2MoO_4 aqueous solution (pH = 11). The triple-quantum MQMAS spectrum of $[(NH_4)_6Mo_7O_{24}] \cdot 4H_2O$ was acquired with a simple two-pulse quadrupolar echo scheme with a 12 phase cycle and rotor synchronized detection in the first dimension (10 kHz). The pulse durations were set empirically to 8.5 and 2.85 μs for the first and the second pulse ($\Omega_I/2\pi \sim$ 40 kHz). These values maximized the observed signal. A total of 8400 scans were accumulated with a recycle time of 0.5 s. Data processing included zero filling, shearing, and scaling according to convention C_Z.[25]

Modeling. The central bands (CB) of the one-pulse spectra were fitted assuming a central transition (CT) second-order quadrupolar line shape using the DMFIT program.[26] When necessary, more complex models of the CB and the spinning sidebands (SSB), including the pulse, the chemical shift anisotropy, and the satellite transitions (ST), were executed with the SIMPSON program.[27]

DFT Calculations. The theoretical calculations are based on DFT and, more specifically, on the use of the generalized gradient approximation of Perdew et al.[28] with full potential (linearized) augmented plane wave + local orbitals (L/APW+lo),[29] as implemented in the WIEN2k code.[22] In this method, the unit cell is partitioned between spheres centered on the atomic sites and the interstitial region. In the latter, plane waves are used as basis functions, whereas in the former, an atomic-like expansion into numerical radial functions times spherical harmonics (up to $l = 10$) is used. Each partial wave is matched in value at the sphere boundary to the corresponding plane wave with a coefficient $A_{lm}(\mathbf{k}_n)$. The radial functions are solutions of the radial Schrödinger equation for given angular momentum and fixed energy, E_l. The necessary flexibility of the basis is gained by additional "local orbitals" (lo), which consist of a linear combination of the same radial function and its energy derivative. They are not matched to any plane wave but are constrained to have zero value at the sphere boundary.

Sphere sizes of 1.8, 1.4, and 2.4 bohr for Mo, O, and A spheres (A = Ca, Ba, Zn, Pb), respectively, were used. Basis of 6156, 7670, 81276, and 7010 plane waves (corresponding to $R_{min}K_{max} = 7.0$) were used, and the Brillouin zone (BZ) integration was done with 12, 52, 9, and 52 *k*-points in the irreducible BZ of $AMoO_4$ crystal structures with A = Ca, Ba, Zn, and Pb, respectively.

The full electric field gradient (EFG) tensor was calculated from the total self-consistent charge density $\rho(r)$ in the crystal without further approximations. For example, the principal EFG component, V_{zz}, was obtained using

$$V_{zz} \approx \int \frac{\rho(r) Y_{20}(\hat{r})}{r^3} \mathrm{d}\vec{r} \qquad (1)$$

where Y_{20} is a spherical harmonic with $l = 2$ and $m = 0$. Because all electrons are taken into account, the charge redistribution is automatically achieved in the self-consistent field procedure, and thus, no additional Sternheimer (anti) shielding factors are needed to explain the EFG. This method has been successfully applied to many types of solids[30−32] and has usually led to values concording with the experimental ones within 10−20%. The quadrupole coupling constant C_Q was computed using

$$C_Q = eQV_{ZZ}/h \qquad (2)$$

A quadrupole moment Q for ^{95}Mo equal to −22 mB is taken from Pyykkö.[33] Because NMR is not sensitive to the sign of C_Q at ambient temperature, absolute values of C_Q have been considered.

Results and Qualitative Interpretations

1. Tetrahedral Coordination Compounds. In monomolybdates of general formula A_nMoO_4, the oxygen packing and the coordination number of the A cation vary, giving rise to a wide range of structures stable at STP.[34] Nevertheless, the basis for all atomic arrangements remains an alternating array of distorted MoO_4^{2-} tetrahedra and cation polyhedra. MoO_4^{2-} units are never adjacent and are linked to the cation polyhedra only by sharing vertices. If the structures are all resolved, only a few have been refined by neutron diffraction, and the exact oxygen positions are rarely known with precision (Table 1). This renders the chemical shift and quadrupole NMR data reported in Table 2 all the more informative, albeit sometimes difficult to interpret. Table 2 also lists for reference purposes previous NMR studies at lower fields when existing. It additionally reproduces Mo−O bond lengths and angular deviation in order to qualitatively apprehend the level of distortions from the ideal T_d symmetry of the tetrahedral molybdenum coordination shell.

1.1. $A(I)_2MoO_4$ Molybdates. Monomolybdates of alkali cations constitute an interesting series for epitomizing the sensitivity of ^{95}Mo NMR to its local environment. Li_2MoO_4 crystallizes as a distorted analogue of phenakite (trigonal space group $P3_2$, no. 145) in which the lithium cation is four coordinated and occupies the tetrahedral holes of the close-

TABLE 1: Structural References for the Monomolybdate Samples

sample	structural type	cation radius (Å)	MoO_4^{2-} units (no.)	structural data from
		$A(I)_2MoO_4$		
Li_2MoO_4	phenakite	0.73	VI	XRD[35]
α-Na_2MoO_4	distorted spinel	1.16	I	powder XRD[36,37]
α-K_2MoO_4		1.52	I	single crystal XRD[38]
Cs_2MoO_4	isotypic to β-K_2SO_4	1.81	I	powder XRD[39]
$Na_2MoO_4.2H_2O$	layered		I	single crystal XRD[40]
$(NH_4)_2MoO_4$ *m*S60	isotypic to α-K_2MoO_4		I	powder XRD[41]
$(NH_4)_2MoO_4$ *m*P60			I	powder XRD[41]
		$A(II)MoO_4$		
$CaMoO_4$	scheelite	1.26	I	neutron[42]
$PbMoO_4$	scheelite	1.43	I	neutron[43]
$BaMoO_4$	scheelite	1.56	I	neutron[44]
α-$ZnMoO_4$		0.88	III	single crystal XRD[45]

TABLE 2: NMR Results for the Monomolybdate Samples

sample	Mo−O spread (Å)	O−Mo−O Δ (°)[a]	δ_{iso} (ppm)	C_Q (MHz)	h	LB (Hz)	recycle time (s)	ref NMR
			$A(I)_2MoO_4$					
Li_2MoO_4								
Li(1)	1.738−1.796	2.9/−3.0	−26	1.26	0.6	100	100	16
Li(2)	1.723−1.802	2.2/−1.5						
Li(3)	1.709−1.819	4.8/−4.4						
Li(4)	1.712−1.827	6.2/−3.5						
Li(5)	1.739−1.828	5.1/−2.7						
Li(6)	1.731−1.812	2.1/−3.1						
α-Na_2MoO_4		0	−33.5	0		33	10000	8, 16
α-K_2MoO_4	1.74−1.78	3.4/−1.7	−17	1.27	0.6	300	100	16, 18
Cs_2MoO_4	1.777−1.765	0	−21	0		100	100	16, 18
$Na_2MoO_4{\cdot}2H_2O$	1.753−1.788	2.3/−1.2	10	1.2	0.7	500	1000	11, 17
$(NH_4)_2MoO_4$ *m*P60	1.758−1.767	3.1/−2.0	31	3.21	0.85	100	100	
$(NH_4)_2MoO_4$ *m*S60	1.759−1.764	2.5/−2.1	−20	2.6	0.4	100	100	
			$A(II)MoO_4$					
$CaMoO_4$	1.739	11.9/−5.6	46	2.94	0.1	100	20	16
$PbMoO_4$	1.774	3.4/−1.7	118	2.03	0.1	100	10	16, 17
$BaMoO_4$	1.765	2.3/−1.2	−35	1.68	0.1	100	100	16
α-$ZnMoO_4$								
Mo(1)	1.737−1.783	2.8/−4.1	−40	2.47	0.6	200	100	
Mo(2)	1.739−1.810	2.5/−2.1	−165	1.15	0.65	200		
Mo(3)	1.707−1.842	3.1/−2.0	−81	2.04	0.6	200		

[a] Maximum positive and negative deviations from the 109.5° angle of an ideal tetrahedral symmetry.

packed array of oxygen atoms in regular alternation with molybdenum. In sodium molybdate, the bulkier cation is six coordinated, but the oxygen atoms remain arranged in a close-packed cubic array, and the crystal adopts a spinel structure (space group $Fd\bar{3}m$, no. 227) with a small trigonal distortion. When the cation size is further increased as for K and Cs, it forms larger polyhedra (trigonal prismatic for K), which dominate the structure: The oxygen atoms do not form a close-packed array anymore. Alternating alkali atoms and Mo tetrahedral construct looser structures (as compared to the spinel structure of phenakite) in α-K_2MoO_4 (monoclinic space group $C2/m$, no. 12) and Cs_2MoO_4 (orthorhombic space group *Pnam*, no. 62). The Mo coordination is much more regular in the Cs than in the K molybdate, forming a tetrahedron very close to ideality with an angular deviation of less than a degree and Mo−O bond distances varying within 0.01 Å. Good representations of these structures can be found in a recent review of A_2MO_4 oxometalates crystal chemistry.[34]

Despite the diversity of structures, all of the alkali metal molybdates studied resonated within a limited isotropic chemical shift range (δ_{iso}) between −17 and −34 ppm (Figure 1 and Table 2). In theory, the cubic symmetry of the oxygens around the Mo sites is not reduced by the trigonal distortion in spinels allowing for a null electrical field gradient around the Mo atoms in α-Na_2MoO_4. Indeed, a nearly perfect, narrow (33 Hz), Lorentzian ^{95}Mo resonance was observed in this molybdate (note that this is not true for the Na sites, which are predicted to be affected by the distortion and for which the measurement of the EFG by ^{23}Na NMR is a well-known case study).[8] On the contrary, the CB resonance of the Li and K monomolybdate had typical CT second-order quadrupole dominated shapes with equal coupling (C_Q) and asymmetry (η) parameters reflecting on the similar distortion of the Mo tetrahedral coordination. One-pulse ^{95}Mo NMR did not distinguish the six Mo sites in Li_2MoO_4. In the literature, the quadrupole coupling has been reported as null for all anhydrous alkali molybdates by Mastikhin et al (Li, Na, Cs)[16] under 7 T and Edwards et al. (K, Cs)[18] under 9.4 T with the exception of α-K_2MoO_4 for which the former authors measured a C_Q of 1.3 MHz. However, the spectacular gain in breadth, signal intensity, and resolution obtained here under 19.6 T revealed the quadrupole coupling of ^{95}Mo for both K and Li molybdates. Also, being more accurately adjusted for the second-order quadrupolar shift, the present δ_{iso} values obtained at 19.6 T could be considered more reliable.

$(NH_4)_2MoO_4$ occurs in two polymorphic forms *m*S60 and *m*P60 with different arrangements of the polyhedra by hydrogen bonds.[41] XRD revealed that both polytypes coexisted in our sample, and indeed, two distinct resonances were apparent in the ^{95}Mo spectrum (Figure 2). Tentatively, the resonance with the strongest quadrupole coupling and asymmetry was attributed

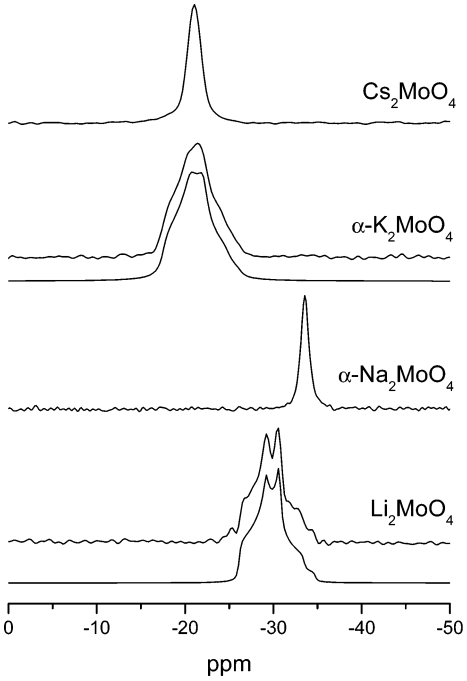

Figure 1. ^{95}Mo MAS NMR of powders of anhydrous alkali metal monomolybdates in their STP stable phases. The top traces are the one-pulse spectra obtained at 54 MHz (19.6 T). The second-order quadrupolar models of the CB of the CT shown on the lower traces when applicable were calculated using the values given in Table 2. Number of scans: 68 (Li), 8 (Na), 32 (K), and 80 (Cs).

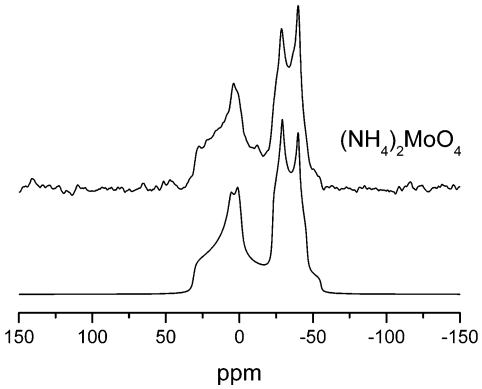

Figure 2. ^{95}Mo MAS NMR of ammonium molybdate in a powder mixture of the two STP stable polytypes *m*P60 and *m*S60. The top trace is the one-pulse spectrum obtained at 54 MHz (19.6 T). The second-order quadrupolar model of the CB of the CTs shown on the lower trace was calculated using the values given in Table 2. Number of scans: 392.

to the Mo nuclei in the structure with the O−Mo−O bond angles deviating the most from the ideal 109.5° tetrahedral angle (*m*P60). Because α-K_2MoO_4 and *m*S60 $(NH_4)_2MoO_4$ are isotypic, it was not surprising that the Mo had a similar chemical shift in both species (−17 and −20, respectively), even though the quadrupole parameters differed significantly. This difference between α-K_2MoO_4 and *m*S60 $(NH_4)_2MoO_4$ and, a fortiori, *m*P60 $(NH_4)_2MoO_4$ demonstrated the sensitivity of the NMR spectra on the presence of hydrogen bonds, either directly through the polarization of the oxygen electrons or through the structural changes they infer. This was confirmed by the spectra of sodium molybdate [$Na_2MoO_4 \cdot 2H_2O$ crystals (orthorhombic space group *Pbca*, no. 61) that are composed of alternating layers of MoO_4^{2-} and H_2O bridged by interlinking Na^+ and hydrogen bonds][40]at different hydration levels (Figures 1 and 3). Moisture induces structural changes, which directly affected

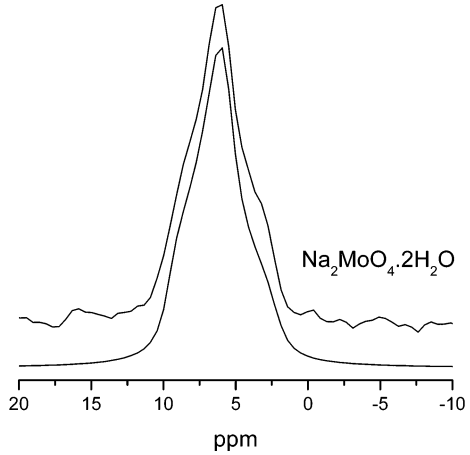

Figure 3. ^{95}Mo MAS NMR of sodium molybdate dihydrate powder. The top trace is the one-pulse spectrum obtained at 54 MHz (19.6 T). The second-order quadrupolar model of the CB of the CT shown on the lower traces was calculated using the values given in Table 2. Number of scans: 8.

the ^{95}Mo spectra. Although the Mo coordination remains formally unchanged, the δ_{iso} of Na_2MoO_4 shifts from −33.5 to 10 ppm upon the formation of the dihydrate and back to 0 ppm for the fully hydrated form (the solvated reference). This strong dependence upon the water content of the sample probably explains the discrepancies of the data obtained by Eichele[11] and Edwards[17] at the same applied magnetic field (9.4 T).

1.2. A(II)MoO₄ Molybdates. A(II)MoO_4 ternary oxides generally crystallize at STP in the same scheelite type structure (tetragonal space group I_1/a, no. 88) where each Mo is identically coordinated to four equivalent O in approximate tetrahedral symmetry (Table 1). In turn, all O are coordinated to two A cations and one Mo. The A^{2+} cations form scalenohedron (eight coordinated). $CaMoO_4$, $BaMoO_4$, and $PbMoO_4$ adopt a scheelite structure and have been structurally refined by neutron diffraction. As a result, the oxygen surrounding of the molybdenum is precisely known in each of these compounds. $ZnMoO_4$ can form a wolframite structure where Mo is six coordinated, but in the STP stable phase, α-$ZnMoO_4$ (triclinic space group $P\bar{1}$, no. 2) Mo is again four coordinated although with a much more complex atomic arrangements than in scheelite. There are three different Mo tetrahedral sites where O is shared with one or two Zn polyhedron (distorted octahedral and square pyramids). Each Mo(1) and Mo(2) has one O shared with two Zn polyhedra. Mo(3) has two.

The apparent simplicity of the scheelite structure is made possible by the strong distortion of the MoO_4^{2-} tetrahedron. It resulted in a wider chemical shift range than for the A(I)$_2MoO_4$ samples: $PbMoO_4$ and $BaMoO_4$ resonated 153 ppm apart. Furthermore, more severe second-order broadening was observed. However, all surrounding oxygens being equivalent, the asymmetry parameter remained small as compared to what was measured in the A(I)$_2MoO_4$ compounds. This resulted in characteristic quadrupolar line shapes with well-marked edge singularities allowing an unambiguous determination of the quadrupole parameters (Figure 4). At the field and pulse power used, all of the CB resonances could be fully interpreted in terms of CT quadrupole interaction neglecting chemical shift anisotropy and contributions from the STs. To illustrate this point, the modeled line shape for $CaMoO_4$ obtained with DMFIT (quadrupolar second-order CT only) was compared to the one obtained with the same parameters with SIMPSON, taking into account the spinning speed, the excitation pulse, and the contribution from all transitions. It was clear that considering

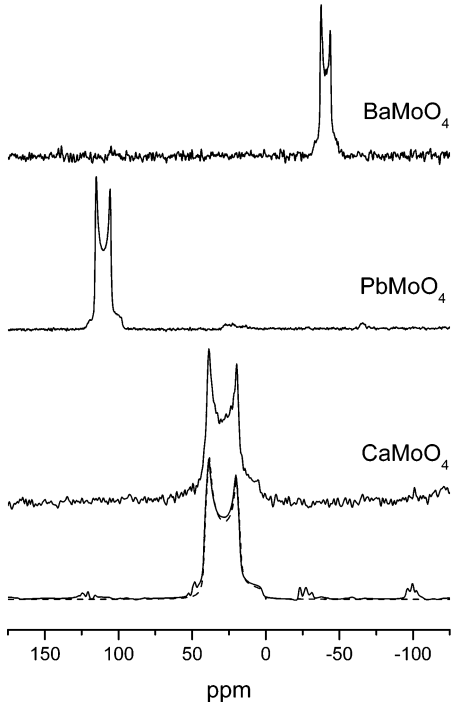

Figure 4. ^{95}Mo MAS NMR of powders of A(II)MoO_4 monomolybdates with scheelite type phases. The one-pulse spectra were obtained at 54 MHz (19.6 T). The traces below the spectrum of $CaMoO_4$ are models calculated using the values given in Table 2: dashed line, CT only using DMFIT; solid line, full spectrum and all transitions considering the pulse using SIMPSON. Number of scans: 440 (Ca), 160 (Pb), and 104 (Ba).

only the CB of the CT is sufficient for determining the NMR interactions parameters. The inclusion of the STs resulted only in a minute improvement of the model by better describing the low field side of the CB and evidently the SSBs. The simulation of the SSBs could certainly be improved by including a small chemical shift anisotropy, but they were lost in the noise for the most part. The NMR parameters obtained here were in reasonable agreement with previous works[16,17] as far as the scheelite structures were concerned. Again, as for the $A(I)_2MoO_4$ results, the isotropic chemical shift obtained here at a higher field can be expected to be more accurate, as the quadrupolar second-order shift of the CT, inversely proportional to the B_0 field, is reduced while the chemical shifts, directly proportional to B_0, increase. For example, a value of 46 ppm was obtained at 19.6 T when it was previously estimated at 35 ppm from a spectrum obtained at 7 T.[16]

The spectrum of α-$ZnMoO_4$ is in general agreement with what can be expected from its structure (Figure 5). With the tetrahedron in α-$ZnMoO_4$ being constituted of nonequivalent O, the asymmetry parameter was considerably higher than in the scheelite structure. Also, the occurrence of three structurally dissimilar tetrahedra translated into three distinct resonances with significantly different quadrupole couplings. Their assignment is postponed to the discussion section (below).

1.3 $Al_2(MoO_4)_3$. This compound is of interest to heterogeneous catalysis, because it develops on alumina-supported Mo-based catalysts. The sample used in this study was the low temperature form (monoclinic space group $P2_1/a$). Alternating AlO_6 octahedra and MoO_4 tetrahedra sharing vertices form a three-dimensional, flexible, open network. Neutron diffraction reveals a small level of distortion resulting in four dissimilar Al and six dissimilar Mo.[46] The Mo−O bond distance has a spread from 1.698 to 1.812 Å. The resolution of all of the

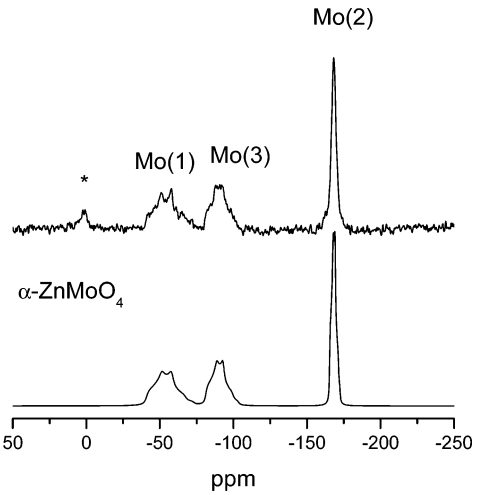

Figure 5. ^{95}Mo MAS NMR of α-$ZnMoO_4$ monomolybdate powder. The top trace is the one-pulse spectrum obtained at 54 MHz (19.6 T). The star marks a SSB. The second-order quadrupolar model of the CB of the CTs shown on the lower trace was calculated using the values given in Table 2. Number of scans: 256.

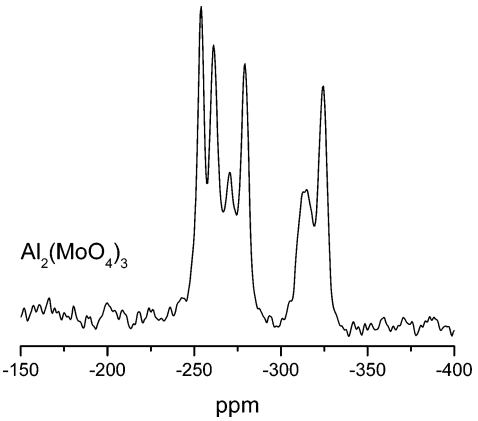

Figure 6. One-pulse ^{95}Mo MAS NMR of α-$Al_2(MoO_4)_3$ powder obtained at 54 MHz (19.6 T). Number of scans: 48. Recycle time: 60 s. The six Mo sites result in six maxima at −254, −261, −270, −279, −314, and −325 ppm.

expected[27]Al resonances represents one of the tours de force accomplished by DOR NMR.[47] Yet, attempts to resolve the nonequivalent MoO_4^{2-} units by ^{95}Mo at moderate fields have failed. Under 9.4 T, Edwards[17] observed only one resonance centered at −300 ppm, and under 11.7 T, Han[20] observed two ca. −270 and −330 ppm, both with a limited signal-to-noise ratio of 3 to 4. The one-pulse spectrum acquired at 19.6 T showed the six resonances expected from α-$Al_2(MoO_4)_3$, some of them fully resolved (Figure 6). This constituted a good example of the improvement to be expected by using high fields. The resonances were, however, featureless, thus preventing accurate estimation of the quadrupole coupling.

2. Octahedral Coordination Compounds. The extension of the coordination of Mo to its maximum of six upon acidification involves the addition of octahedra into compact polyanionic structures (Table 3).[1] However, the well-known ability of the Mo atom to form double bonds with unshared oxygens by $d_\pi-p_\pi$ interaction shortens the corresponding Mo−O distances and thus creates a significant deviation of MoO_6 units from ideal O_h octahedral symmetry.[48] Moreover, the oxygens of the exterior layer of the compact polymolybdate anions are strongly polarized toward the highly charged Mo^{6+}. Exerting a strong attraction, they significantly displace the Mo atom off-center, distorting further the octahedral symmetry. This dependence of

TABLE 3: Structural References for the Octahedral Structures

sample	structure	MoO_6 units (number)	O types (number)	approximate MoO_6 symmetry	structural data from
Ba_2CaMoO_6	perovskite	I	6 O_t	O_h	powder XRD[49]
$(NtBu_4)_2Mo_6O_{19}$	lindqvist	III	1 O_t, 4 μ_2, 1 μ_6 (O_i)	C_{4v}	single crystal XRD[50]
$[(NH_4)_6Mo_7O_{24}]$ $4H_2O$	evans	III	type I: 2 O_t, 2 μ_2, 1 μ_3, 1 μ_4 type II: 2 O_t, 3 μ_2, 1 μ_4 type III: 2 μ_2, 2 μ_3, 2 μ_4	C_{2v}	single crystal XRD[51]
α-MoO_3	layered	I	1 O_t, 2 μ_2, 2 μ_3, 1 μ_4	C_S	single crystal XRD[52]

TABLE 4: NMR Results for the Octahedral Structures

sample	Mo−O spread (Å)	O−Mo−O Δ (°)[a]	δ_{iso} (ppm)	$C_{Q\eta}$ (MHz)	LB (Hz)	Δ_{aniso} (ppm)	recycle time (s)
Ba_2CaMoO_6	1.86	0	168.5	0	65		1000
$(NtBu_4)_2Mo_6O_{19}$	O_t 1.68 μ_2 1.86−2.00 μ_6 (O_i) 2.31−2.32	O_t-μ_2 11.9/14.8 O_t-μ_6 −12.1/−14.8 μ_{2t}-μ_2 −7.2/1.1	112	2.7	600	−400	20
$[(NH_4)_6Mo_7O_{24}]\cdot 4H_2O$	type I: O_t 1.72 μ_2 1.94−1.97 μ_3 2.29 μ_4 2.16	−18.2/15.3	29	0.9	5000		2
	type II: O_t 1.75 μ_2 1.92−2.53 μ_4 2.16	−20.9/15.2	44	2.9	200		
	type III: μ_2 1.74 μ_3 1.90 μ_4 2.25	−13.5/5.5	205	3.0	400		

[a] Maximum positive and negative deviations from the 90° angle of *cis*-oxygens in an ideal octahedral symmetry.

TABLE 5: ^{95}Mo NMR Parameters Derived from MoO_3 Spectra

study	B_0 (T)	δ_{iso} (ppm)	C_Q (MHz)	η_Q	Δ_{aniso} (ppm)	η_{CS}
Mastikhin et al.[16]	7	−150	2.4			
		60	1.8			
Edwards et al.[17]	9.4		3.49	0.99	167	0.96
Han et al.[20]	11.7	∼−90				
Bastow[13]	9.4	−65	2.85	0.32		0.78
this study	19.6	−73	2.8	0.3	260	0.85

local symmetry on the degree of sharing of the oxygen suggests a rationalization of the first Mo coordination shell in terms of terminal (O_t), internal (O_i), and bridging (μ_2−μ_6) oxygens.

The spectral characteristics of octahedral Mo species differed significantly from the ones of tetrahedral monomolybdates (Tables 4 and 5). First, they spread over a wide chemical shift range (from 200 to −100 ppm), encompassing the somewhat narrower tetrahedral range: IV and VI coordination cannot be distinguished on chemical shift alone. Second, they exhibited less distinctive line shapes. Indeed, when compared to the tetrahedral Mo environment of monomolybdates, all based on isolated MoO_4^{2-} units, the different possible edge-sharing arrangements of MoO_6^{6-} octahedra result evidently in a larger diversity of environments but also concomitantly in a multiplicity of bond angles and distances within the same octahedron.

2.1. Ba_2CaMoO_6. The Ba/Ca molybdate is atypical in the sense that in this near-perfect perovskite structure (cubic space group *Fm*3*m*, no. 225) Mo occupies the center of a regular isolated octahedron. The EFG is null by symmetry, and accordingly, the ^{95}Mo MAS NMR was narrow and showed no hint of a quadrupolar line shape (Figure 7).

2.2. MoO_3. The industrial importance of MoO_3 ensures that it figures in all comprehensive solid state ^{95}Mo studies of oxides.

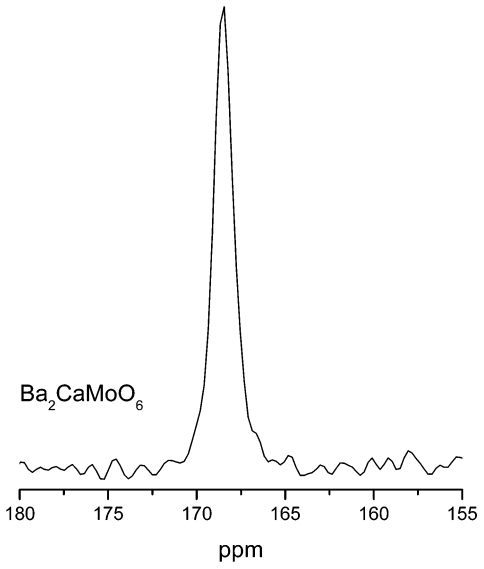

Figure 7. One-pulse ^{95}Mo MAS NMR of Ba_2CaMoO_6 powder obtained at 54 MHz (19.6 T). Number of scans: 8.

The lamellar structure of α-MoO_3 is commonly described with octahedral Mo, but the Mo−O distances are such that it can be alternatively represented using tetrahedra. It can therefore be taken as representative of an intermediate between octahedral and tetrahedral coordination. Indeed, its spectrum, being dominated by the quadrupole interaction, reproduced the general features observed for tetrahedral species, except for a small contribution of the chemical shift anisotropy evident from the SSBs (Figure 8). The values reported in the literature for the orthorhombic form (the thermodynamically stable form α-MoO_3, space group *Pnma*, no. 62) are rather conflicting with regards

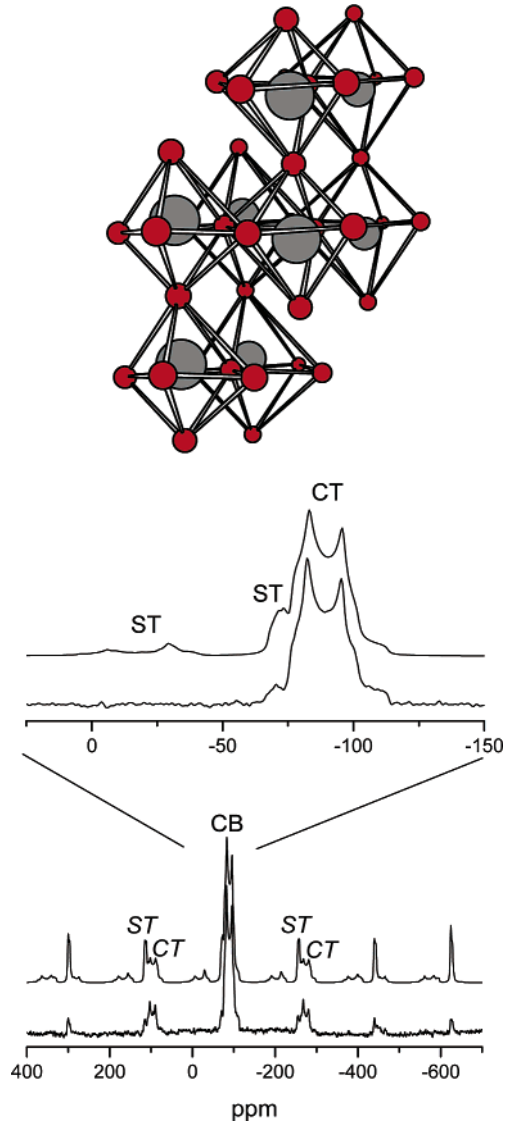

Figure 8. ^{95}Mo MAS NMR of a powder of orthorhombic α-MoO_3. The lower trace is the one-pulse spectrum obtained at 54 MHz (19.6 T). The upper trace was generated by SIMPSON using the values given in Table 5. Number of scans: 400. Recycle time: 18 s.

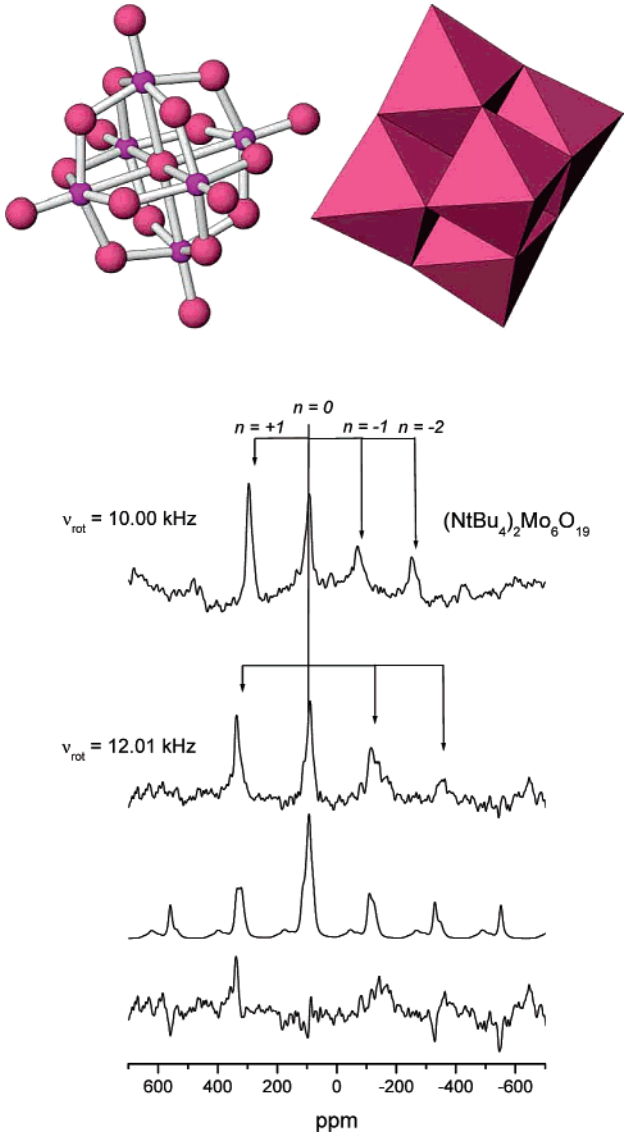

Figure 9. One-pulse ^{95}Mo MAS NMR of $(NtBu_4)_2Mo_6O_{19}$ powder obtained at 54 MHz (19.6 T) with different spinning rates. The arrows position the *n*th spinning harmonics of the CB and do not exactly coincide with the SSB pattern. A model calculated with SIMPSON with ν_{rot} 12 kHz and the parameters of Table 4 is presented with the residual (experimental minus calculated) underneath. The signal-to-noise was not good enough to extract the asymmetry parameters and the relative orientation of the chemical shift relative to the quadrupole tensor. Arbitrarily, the asymmetry parameters were both set to 0.75 and the angles were set as coincidental for the sake of comparison. The residual (experimental minus model) showed that the intensity of the +1 SSB is systematically underestimated in the one site model. Number of scans: 320.

to quadrupole as well as chemical shift parameters.[13,16,17,20] The spectrum obtained under 19.6 T was modeled as follows. First, the quadrupole parameters were extracted by fitting the CB, considering only the second-order quadrupolar powder line shape singularities of the CT using DMFIT. However, the line shape generated in this manner did not account for the low field shoulder of the CB, and the relative intensities of the singularities were incorrect. Therefore, a full spectrum was generated using SIMPSON, including chemical shift anisotropy, which allowed for a satisfactory modeling of the CB and SSB for the CT as well as for the STs (the relative intensities of the CT and STs contributions to the spectrum were incorrect since the spectrum was generated assuming an even excitation of all of the transitions, which is definitely not the case for a $\pi/6$ pulse). Table 5 compares the values so obtained with the literature data. The high field spectrum of this study appeared most compatible with the data and DFT calculation of Bastow.[13,14]

2.3. $(NtBu_4)_2Mo_6O_{19}$. The Lindqvist structure exemplifies how, even in regular arrangements, the occurrence of a terminal oxygen implies a displacement of the Mo from the center of the octahedron and a strong departure from O_h symmetry. The $Mo_6O_{19}^{2-}$ anion consists of six fused octahedra sharing a common vertex to form a "super-octahedron". One central oxygen (O_i) is bound to all the Mo and can therefore be termed a μ_6. The MoO_6 units are nearly identical with one terminal oxygen (O_t) and one μ_6 internal oxygen in trans positions. The four remaining ones bridge two Mo and so constitute μ_2 oxygens. The Mo−O_t bond is shorter (1.68 Å) than the opposite Mo−O(μ_6) one (2.32 Å). The resulting ^{95}Mo CB resonance was broad (600 Hz) with a strong SSB pattern extending over 40 kHz (Figure 9). The CB had no distinctive line shape, but close inspection of the full spectrum revealed a systematic downfield shift difference of 0.9 ± 0.1 kHz between the center of the SSB pattern and the CB position. Assuming that the SSBs

originate from the quadrupole interaction on the ST, this shift difference can result from the second-order quadrupolar isotropic frequencies ($\nu^{(2)}_{\langle m,m-1\rangle}$) for the central ($m = 1/2$) and inner satellite ($m' = 3/2$) transition. Consequently, the quadrupole frequency (ν_Q) and the quadrupole coupling constant (C_Q) was calculated according to:

$$\nu_Q = \sqrt{\frac{10}{3}(\nu^{(2)}_{\langle m,m-1\rangle} - \nu^{(2)}_{\langle m',m'-1\rangle})\frac{\nu_0}{[m(m-1) - m'(m'-1)]}\frac{1}{1+\frac{\eta^2}{3}}} \quad (3)$$

$$C_Q = \frac{2I(2I-1)\nu_Q}{3} \quad (4)$$

where ν_Q is in kHz, $\nu^{(2)}_{\langle m,m-1\rangle}$ is in Hz, and the Larmor frequency ν_0 is in MHz. The asymmetry parameter (η) being undetermined, one gets only the commonly used parameter

$$C_{Q\eta} = C_Q\sqrt{\frac{\eta^2}{3}+1} = \frac{2I(2I-1)}{3}\sqrt{\frac{10}{3}(\nu^{(2)}_{\langle m,m-1\rangle} - \nu^{(2)}_{\langle m',m'-1\rangle})\frac{\nu_0}{[m(m-1) - m'(m'-1)]}} \quad (5)$$

For ^{95}Mo ($I = 5/2$) at $\nu_0 = 54.05$ MHz, the measured shift difference of 900 Hz led to

$$C_{Q\eta} = 2.7 \pm 0.2 \text{ MHz}$$

From this value, a true isotropic chemical shift of 112 ppm could be obtained while the chemical shift anisotropy could be estimated at -400 ± 100 ppm from the spread of the SSB pattern. These values could be questioned as they differed from the ones previously reported at a lower field.[17] Nevertheless, they were supported by two facts. First, published theoretical estimations of the local charge on the molybdenum predicted a chemical shift of 122 ppm.[53] Second, it was possible to perform a simulation reproducing the main features of the spectrum, although the low signal-to-noise ratio prevented further adjustments of the asymmetry parameters and of the angles of the interaction tensors. In any case, the intensity of the $n = +1$ SSB was systematically underestimated in the model assuming only one Mo site. Edwards and co-workers reported a similar observation: the "mirror image" nature of their simulation in comparison to the experimental spectrum.[17] They attribute it to a compositional impurity of their sample, but the reproducibility of this result suggests an intrinsic explanation. Indeed, the bridging μ_2s are not exactly equidistant from the flanking Mo atoms lowering the symmetry below C_{4v} and three slightly dissimilar Mo can be distinguished with μ_2−Mo bond lengths varying between 1.86 and 2.00 Å.[50] It is possible that the experimental spectrum might actually be a complex superposition of sites with different interaction tensors.

2.4. $(NH_4)_6Mo_7O_{24}\cdot 4H_2O$. Hexaammonium heptamolybdate, stable at acidic to near neutral pH, is a precursor of catalysts prepared by impregnation and, therefore, a compound of practical importance. It adopts the Evans structure[51] in which three octahedra are aligned with four more attached forward, two above and two below, in a "butterfly" arrangement. As a result, there are three dissimilar Mo: the one in the central octahedron of the line (type III), the two at the end of the line

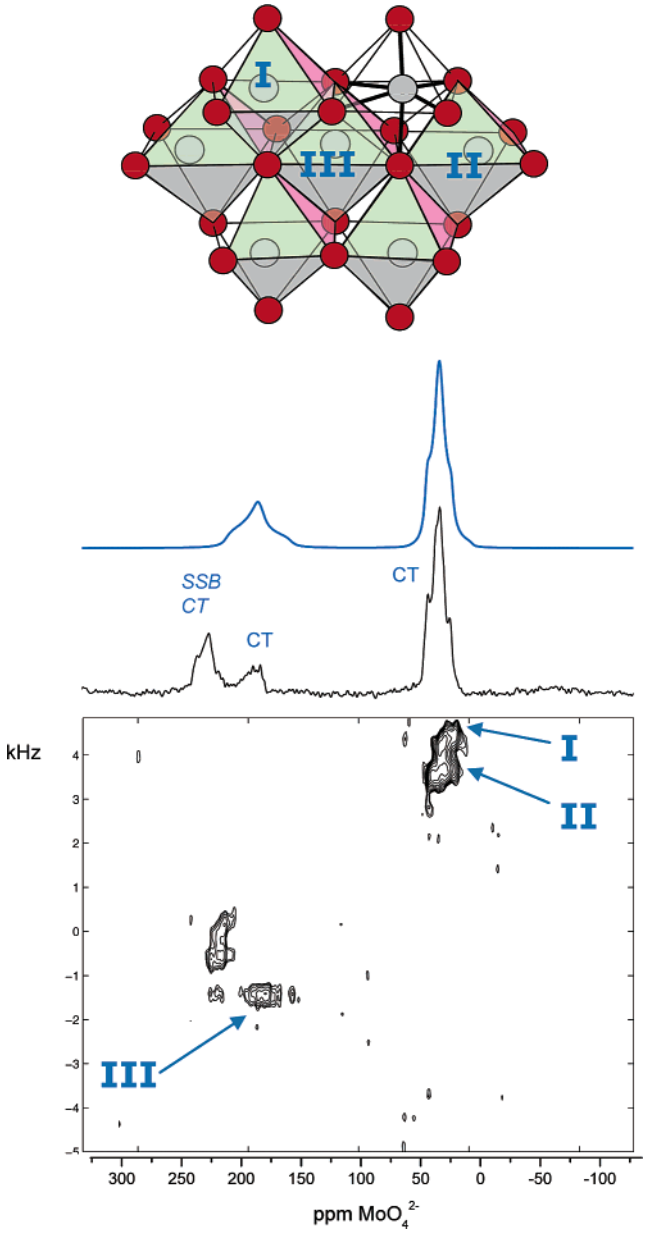

Figure 10. One-pulse and 3Q-MAS ^{95}Mo spectra of $[(NH_4)_6Mo_7O_{24}]\cdot 4H_2O$ powder obtained at 54 MHz (19.6 T). Number of scans for the one-pulse spectra: 4000.

(type II), and the four forward ones (type I). Because only two resonances were resolved around 30 and 170 ppm, a multidimensional 3Q-MAS experiment was attempted to test the potential of this method for low γ nuclei at high fields (Figure 10). Beyond the general issue of sensibility, the MQMAS of low γ nuclei is particularly challenging. To generate multiple-order coherences, a strong radio frequency field B_1 is required to compensate for the low gyromagnetic ratio γ since the efficiency of the pulse scales according to $\gamma B_1/2\pi$. Multiple coherences were nevertheless generated here with a simple two pulse scheme revealing the composite nature of the upfield resonance. The $C_{Q\eta}$ and the isotropic chemical shift were extracted from the center of gravity of the resonances in the *F1* and *F2* dimensions.[25] The main upfield resonance appeared composite, consisting of two resonances of similar chemical shift but different $C_{Q\eta}$. The MQMAS results were further used as constraints for the fit of the one-pulse spectrum: The result was satisfactory, but it was necessary to considerably broaden the resonance at 29 ppm, and it was not possible to discriminate

between values of η. From the shape of the 205 ppm resonance, the η could be closer to unity and was arbitrarily modeled as such. On the basis of its intensity, this resonance was attributed with some confidence to the type III molybdenum. Types I and II molybdenum have the same number of terminal oxygen ligands and can be expected to have similar charge densities and chemical shifts. It has been proposed to assign the resonances according to quadrupole constant and to average angles between the bonds of *cis*-oxygens with the central molybdenum.[17] It is not clear, however, how much such an average truly reflects the degree of distortion of the octahedral geometry and, consequently, the EFG. Speculatively, in the absence of exact charge density and gradient at the molybdenum, it seemed preferable to assume that the type II having the larger spread in bond lengths and angles would relate to the resonance with the largest $C_{Q\eta}$.

Discussion

The chemical shift results from the sum of a diamagnetic and a paramagnetic contribution. While the calculation of the diamagnetic shift is relatively easy, it is commonly accepted that beyond the third row elements, the increased positive charge at the nucleus is responsible for extensive relativistic effects complicating the calculation of the paramagnetic shift. In an exemplary study of a molybdenum piano stool complex, Bryce and Wasylishen have shown that relativistic and nonrelativistic DFT predictions of the ^{95}Mo paramagnetic chemical shift can differ by an order of magnitude.[21] In molybdates, the relativistic contribution to the shift is likely to be just as significant but much more difficult to predict ab initio, thus rendering any structural interpretation of the chemical shift problematic. It is indeed apparent from the experimental data reported here that the isotropic chemical shifts of ^{95}Mo cannot be used directly to characterize the local structures of molybdates. The chemical shift range for tetrahedral environments is fully included within the spread of the octahedral resonances. Even within a given chemical series, i.e., alkali molybdates, no clear correlation between the chemical shift and the elemental (such as ionic radii) or structural data (such as bond lengths or angles) could be easily derived. In contrast, the quadrupole interaction, whose tensor is directly proportional not to the charge density but to the EFG at the nucleus (eq 2), appears as a more manageable quantity. Probing the symmetry of the electronic environment of the nucleus, it constitutes also a very informative structural probe. However, because of the significant distortion of the MoO_4^{2-} or MoO_6^{6-} polyhedra, deviation from an ideal symmetry cannot be apprehended from a single structural parameter. For instance, as stated above when presenting the MQMAS of ammonium hexamolybdate, the choice of the mean or the standard deviation as an indication of the extent of the EFG is somewhat arbitrary. Furthermore, there is no concordance between the standard deviation from the ideal Mo−O−Mo angles (109.5 and 90° for tetrahedron and octahedron, respectively) and from the mean Mo−O distance. Selecting one or the other criterion for assessing the distortion of the polyhedra leads to conflicting conclusions. The case of α-$ZnMoO_4$ constitutes an exemplifying dilemma: Should the resonance with the highest C_Q be associated to the site with the highest angular [Mo(1)] or lengths [Mo(3)] spread? It therefore appeared that a more comprehensive approach was unavoidable. Consequently, ^{95}Mo quadrupole parameters have been computed using DFT for the A(II)MoO_4 compounds that adopt a scheelite structure (A = Ca, Ba, Pb) as well as for α-$ZnMoO_4$. These compounds present the advantage of having their structure precisely known through single crystals or neutron diffraction data.

TABLE 6: Quadrupole Parameters Computed from DFT

compound	C_Q (MHz)	η_Q
$CaMoO_4$	4.03	0
$PbMoO_4$	2.48	0
$BaMoO_4$	1.84	0
α-$ZnMoO_4$		
Mo(1)	2.85	0.79
Mo(2)	1.29	0.64
Mo(3)	2.08	0.65

Results are reported in Table 6. Because of the point symmetry of the Mo position in the scheelite structure, the quadrupole asymmetry parameter η_Q was null. Computed C_Q values for Mo atoms in $BaMoO_4$ and $PbMoO_4$ agreed well with the experimental data (Table 2). The ^{95}Mo C_Q value computed for $CaMoO_4$ was about 30% higher than the measured one. The same C_Q value was obtained using different computational parameters (basis set and exchange correlation functional). This difference is higher than the one generally accepted between experimental and theoretical values.[30−32] To enlighten this discrepancy, the crystal structure has been relaxed with respect to total energy. Because the optimized crystallographic structure is very close to the experimental one, the C_Q remains unchanged. A possible explanation for this difference could reside in a low frequency dynamic effect on the CT of half-integer quadrupolar nuclei NMR spectra. Such an effect (a few kHz) is known to average out NMR second-order quadrupole effects.[54,55] A partial dynamic averaging leads to an "apparent" C_Q value smaller than the computed one using DFT methods.

Apart from the open case of $CaMoO_4$, the measured coupling constants closely matched the ones derived from the DFT calculations. The same was true for the values obtained for the α-$ZnMoO_4$. Consequently, the downfield resonance was assigned without ambiguity to the Mo(1) tetrahedron and the upfield one to Mo(2).

Following these results, it appeared that in the case of multiple sites compounds, the complexity of the molybdenum environment geometry required such a theoretical analysis for a definite assignment of experimental quadrupole parameters to Mo crystallographic positions. However, DFT calculations could not be carried out for other compounds within a reasonable computational effort because of large unit cells and/or the low space group symmetry of their crystal structures. Compounds with a low precision crystal structure in terms of protons localization could also not be considered for ab initio predictions. This excluded de facto the polymolybdates for which only a qualitative assignment could be performed. It remained that clear fingerprints of the structures were obtained for all compounds. Direct comparison of the high field experimental spectra with simulated one-dimensional line shapes provided a unique determination of the NMR parameters in the case of species having a single Mo(VI) environment (Figures 1−8), supported when possible by DFT calculations. Complementarily, when the existence of unresolved multiple sites precluded such a direct analysis, the use of a high field provided enough sensibility to mobilize efficiently the refined arsenal of modern MAS NMR such as precise SSB analysis or two-dimensional MQMAS experiments.

Conclusions

The usefulness of ^{95}Mo NMR in the solid states as a molecular probe obviously depends on the structural readability of the spectra. NMR parameters may often be correlated with the coordination number, nature of the second coordination sphere, bond angles, or bond lengths. Because of this straight-

forward interpretation, it is a very useful tool for nuclei like ^{27}Al, ^{17}O, or even for 3d transition metals such as ^{51}V. However, the correlation of the quadrupole parameters with the structures, although theoretically evident (eq 1), was practically obscure at first sight for ^{95}Mo. No general trend could be immediately extracted from the NMR quadrupole parameters.

This study confirmed that a rationalization of quadrupole parameters for molybdenum, and probably for most 4d transition metals, requires the in-depth comprehension of the band structures of the compounds provided by DFT calculations from known crystallographic structures. When this is not possible, the improvements linked to high fields provided empirical quadrupolar NMR fingerprints of the structures on a case-by-case basis.

Quantitative identification of the structures present at different stages of preparation of supported HDS catalyst precursors are important not only for designing new synthesis strategies for improved catalysts but even, more modestly, for improving (re)-generation and storage of existing precursors. More generally, the electronic and magnetic properties of d-block transition metal oxides and molybdenum oxides are directly related to their structures. In this respect, this study established the potential of solid state NMR to yield site specific structural information in monomolybdates and isopolymolybdates.

Acknowledgment. Profs. Gédéon, Zanni, and Payen and Dr. Massiot provided the necessary encouragements for this intercontinental enterprise. K.V.R. thanks the NHMFL for a first-time user grant.

References and Notes

(1) Pope, M. T. *Heteropoly and Isopoly Oxometalates*; Springer-Verlag: New York, 1983; Vol. 8.
(2) Payen, E.; Grimblot, J.; Kasztelan, S. *J. Phys. Chem.* **1987**, *91*, 6642−6648.
(3) Cramer, S. P.; Hodgson, K. O.; Stiefel, E. I.; Newton, W. E. *J. Am. Chem. Soc.* **1978**, *100*, 2748−2761.
(4) Lutzenkirchen-Hecht, D.; Frahm, R. *J. Phys. Chem. B* **2001**, *105*, 9988−9993.
(5) Harris, R. K.; Becker, E. D.; De Menezes, S. M. C.; Goodfellow, R.; Granger, P. *Pure Appl. Chem.* **2001**, *73*, 1795−1818.
(6) Siegel, R.; Nakashima, T. T.; Wasylishen, R. E. *Chem. Phys. Lett.* **2004**, *388*, 441−445.
(7) Larsen, F. H.; Skibsted, J.; Jakobsen, H. J.; Nielsen, N. C. *J. Am. Chem. Soc.* **2000**, *122*, 7080−7086.
(8) Lynch, G. F.; Segel, S. L. *Can. J. Phys.* **1972**, *50*, 567−572.
(9) Nolle, A. *Z. Phys. A: Hadrons Nucl.* **1977**, *280*, 231−234.
(10) Edwards, J. C.; Zubieta, J.; Shaikh, S. N.; Chen, Q.; Bank, S.; Ellis, P. D. *Inorg. Chem.* **1990**, *29*, 3381−3393.
(11) Eichele, K.; Wasylishen, R. E.; Nelson, J. H. *J. Phys. Chem. A* **1997**, *101*, 5463−5468.
(12) Proust, A.; Thouvenot, R.; Roh, S. G.; Yoo, J. K.; Gouzerh, P. *Inorg. Chem.* **1995**, *34*, 4106−4112.
(13) Bastow, T. J. *Solid State Nucl. Magn. Reson.* **1998**, *12*, 191−199.
(14) Bastow, T. J. *Solid State Nucl. Magn. Reson.* **2003**, *23*, 116−118.
(15) Machida, N.; Eckert, H. *Solid State Ionics* **1998**, *107*, 255−268.
(16) Mastikhin, V. M.; Lapina, O. B.; Maximovskaya, R. I. *Chem. Phys. Lett.* **1988**, *148*, 413−416.
(17) Edwards, J. C.; Adams, R. D.; Ellis, P. D. *J. Am. Chem. Soc.* **1990**, *112*, 8349−8364.
(18) Edwards, J. C.; Ellis, P. D. *Langmuir* **1991**, *7*, 2117−2134.
(19) Han, O. H.; Lin, C. Y.; Haller, G. L. *Catal. Lett.* **1992**, *14*, 1−9.
(20) Han, O. H.; Lin, C. Y.; Sustache, N.; McMillan, M.; Carruthers, J. D.; Zilm, K. W.; Haller, G. L. *Appl. Catal. A* **1993**, *98*, 195−210.
(21) Bryce, D. L.; Wasylishen, R. E. *Phys. Chem. Chem. Phys.* **2002**, *4*, 3591−3600.
(22) Blaha, P.; Schwarz, K.; Madsen, G. K. H.; Kvasnicka, D.; Luitz, J. *WIEN2k, An Augmented Plane Wave + Local Orbitals Program for Calculating Crystal Properties*; Technische Universität Wien: Wien, 2001.
(23) Winter, M. *WebElements Periodic Table*; http://www.webelements.com/.
(24) Boudias, C.; Monceau, D.; *3.1 ed.*; Divergent S. A.: Senlis, 1998.
(25) Man, P. P. *Phys. Rev. B: Condens. Matter* **1998**, *58*, 2764−2782.
(26) Massiot, D.; Fayon, F.; Capron, M.; King, I.; Le Calve, S.; Alonso, B.; Durand, J. O.; Bujoli, B.; Gan, Z. H.; Hoatson, G. *Magn. Reson. Chem.* **2002**, *40*, 70−76.
(27) Bak, M.; Rasmussen, J. T.; Nielsen, N. C. *J. Magn. Reson.* **2000**, *147*, 296−330.
(28) Perdew, J. P.; Burke, K.; Ernzerhof, M. *Phys. Rev. Lett.* **1996**, *77*, 3865−3868.
(29) Madsen, G. K. H.; Blaha, P.; Schwarz, K.; Sjostedt, E.; Nordstrom, L. *Phys. Rev. B: Condens. Matter* **2001**, *64*.
(30) Schwarz, K.; Blaha, P. *Z. Naturforsch., A: Phys. Sci.* **1992**, *47*, 197−202.
(31) Dufek, P.; Blaha, P.; Schwarz, K. *Phys. Rev. Lett.* **1995**, *75*, 3545−3548.
(32) Blaha, P.; Schwarz, K.; Faber, W.; Luitz, J. *Hyperfine Interact.* **2000**, *126*, 389−395.
(33) Pyykkö, P. *Mol. Phys.* **2001**, *99*, 1617−1629.
(34) Muller-Buschbaum, H. *J. Alloys Compd.* **2003**, *349*, 49−104.
(35) Barinova, A. V.; Rastsvetaeva, R. K.; Nekrasov, Y. V.; Pushcharovskii, D. Y. *Doklady Chem.* **2001**, *376*, 16−19.
(36) Kautt, W. D.; Kruger, H.; Lutz, O.; Maier, H.; Nolle, A. *Z. Naturforsch., A: Phys. Sci.* **1976**, *31*, 351−356.
(37) Bramnik, K. G.; Ehrenberg, H. *Z. Anorg. Allg. Chem.* **2004**, *630*, 1336−1341.
(38) Gatehouse, B. M.; Leverett, P. *J. Chem. Soc. A* **1969**, 849−854.
(39) Gonschorek, W.; Hahn, T. *Z. Kristallogr.* **1973**, *138*, 167−176.
(40) Matsumoto, K.; Kobayashi, A.; Sasaki, Y. *Bull. Chem. Soc. Jpn.* **1975**, *48*, 1009−1013.
(41) Dittmann, M.; Schweda, E. *Z. Anorg. Allg. Chem.* **1998**, *624*, 2033−2037.
(42) Gurmen, E.; Daniels, E.; King, J. S. *J. Chem. Phys.* **1971**, *55*, 1093−1097.
(43) Leciejewicz, J. *Z. Kristallogr.* **1965**, *121*, 158−164.
(44) Nassif, V.; Carbonio, R. E.; Alonso, J. A. *J. Solid State Chem.* **1999**, *146*, 266−270.
(45) Reichelt, W.; Weber, T.; Sohnel, T.; Dabritz, C. *Z. Anorg. Allg. Chem.* **2000**, *626*, 2020−2027.
(46) Harrison, W. T. A.; Cheetham, A. K.; Faber, J. J. *J. Solid State Chem.* **1988**, *76*, 328−333.
(47) Haddix, G. W.; Narayana, M.; Tang, S. C.; Wu, Y. *J. Phys. Chem.* **1993**, *97*, 4624−4627.
(48) Baker, L. C. W.; Glick, D. C. *Chem. Rev.* **1998**, *98*, 3−49.
(49) Chiu, N. S.; Bauer, S. H. *Acta Crystallogr., Sect. C: Cryst. Struct. Commun.* **1984**, *40*, 1646−1647.
(50) Allcock, H. R.; Bissell, E. C.; Shawl, E. T. *Inorg. Chem.* **1973**, *12*, 2963−2968.
(51) Evans, H. T.; Gatehouse, B. M. *J. Chem. Soc., Dalton Trans.* **1975**, 505−514.
(52) Kihlborg, L. *Ark. Kemi* **1963**, *21*, 357−364.
(53) Kazansky, L. P.; Yamase, T. *J. Phys. Chem. A* **2004**, *108*, 6437−6448.
(54) Kristensen, J. H.; Farnan, I. *J. Chem. Phys.* **2001**, *114*, 9608−9624.
(55) Schurko, R. W.; Wi, S.; Frydman, L. *J. Phys. Chem. A* **2002**, *106*, 51−62.